Check for updates

Original Article

Effect of high-temperature exposure on the microstructure and mechanical properties of the Al$_5$Ti$_5$Co$_{35}$Ni$_{35}$Fe$_{20}$ high-entropy alloy

Piotr Bała [a,b,*], *Kamil Górecki* [c], *Wiktor Bednarczyk* [a], *Maria Wątroba* [a], *Sebastian Lech* [a], *Jakub Kawałko* [b]

[a] *AGH University of Science and Technology, Faculty of Metals Engineering and Industrial Computer Science, Al. A. Mickiewicza 30, 30-059 Krakow, Poland*
[b] *AGH University of Science and Technology, Academic Centre for Materials and Nanotechnology, Al. A. Mickiewicza 30, 30-059 Krakow, Poland*
[c] *VSB - Technical University of Ostrava, Institute of Environmental Technology, 17. listopadu 2172/15, 708 00 Ostrava-Poruba, Ostrava, Czech Republic*

ARTICLE INFO

ABSTRACT

Effect of high-temperature exposure on the microstructure and mechanical properties of the Al5Ti5Co35Ni35Fe20 High-Entropy Alloy was studied. High-entropy alloys belong to the group of multi-principal element alloys composed of at least five elements with a concentration between 5 and 35 atomic pct. Despite the multicomponent composition, the goal is to achieve a simple solid solution. The alloy was exposed to a temperature range of 650–900 °C for 168 h (7 days), after hot rolling and air-quenching. After hot rolling the investigated alloy was not fully supersaturated. The application of air cooling caused γ' precipitation, which was uniformly distributed within the microstructure. High-temperature exposure caused the growth of γ' particles. At 700 °C and higher, additional continuous and discontinuous precipitation of γ' was observed. Finally, the microstructure of the investigated alloy consisted of γ matrix and three types of γ' precipitates, i.e. spherical γ' phases with bimodal distribution within the grains and elongated DP γ' phases present at the grain boundaries. The highest mechanical properties were obtained after exposure to 650 °C, which was caused by γ' precipitation. Further increase in temperature decreased the mechanical properties.

1. Introduction

Metallic materials are frequently chosen for structural applications as they have a desirable combination of mechanical characteristics. The final properties of alloys are often the result of not one, but two or more strengthening mechanisms. In this group there are many alloys like stainless steels,

* Corresponding author.
  E-mail: pbala@agh.edu.pl (P. Bała).

high-speed steels, superalloys, and multi-principal element alloys. Usually, they have a complex chemical composition and require advanced production technologies [1–4].

High-Entropy Alloys (HEAs) belong to the group of multi-principal element alloys that are composed of at least five elements with the concentration of each element between 5 and 35 atomic pct. This new group of materials is characterized by several so-called core effects like the high-entropy effect, severe lattice distortion effect, sluggish diffusion effect and cocktail effect. These core effects are responsible for unique properties, including high hardness, thermal resistance, abrasion resistance, and others. One of the most interesting features, resulting directly from the chemical composition of HEAs, is that despite the multicomponent composition, only simple phases form. The goal is to achieve a simple solid solution like face-centered cubic (FCC) or body-centered cubic (BCC) or both (FCC + BCC) [5–7]. It has been reported that in HEA's, solid solutions form rather than intermetallic compounds or other complex ordered phases owing to the high entropy of mixing. The high entropy of mixing stabilized solid solution is very strong, and it is not possible to indicate, which element is the solvent and which ones are solutes [5,6].

HEAs could be in an equilibrium state if sufficiently annealed. However, this is generally a lengthy process in comparison to conventional alloys, due to lower diffusion rates of alloying elements and phase transformation rates [8]. This makes the synthesis of stable HEAs, consisting only of a single phase solid solution, nearly impossible, even in the case of the Cantor alloy, in which authors [9–11] observed σ phase precipitation. However, some authors [12] suggest, that new materials, which are not fully characterized as solutions, should not be disqualified. Often, materials with a high-entropy matrix and additional precipitates possess huge application potential. Therefore, HEAs could have a broad range of chemical compositions, phases, and microstructures and thus generate the desired physical, mechanical, and chemical properties. Certainly, controlling metastable structures to obtain the best performance for specific applications is an important research issue of HEAs [13].

The goal of our research is to investigate the microstructural changes during long term high-temperature exposure of HEA's, which contains elements such as Al or Ti, prone to create intermetallic phases instead of a solid solution. This knowledge is crucial when considering a material for high-temperature applications.

2. Materials and methods

The alloy, with the nominal chemical composition of (at. pct.): Al–5 pct., Ti–5 pct., Co–35 pct., Ni–35 pct., Fe–20 pct., was synthesized in a vacuum melting furnace. Next, a rod-shaped ingot was heat treated in a vacuum furnace for 20 h at 1100 °C to obtain chemical homogeneity throughout the entire volume. Slabs were supersaturated for 1 h at 1200 °C and subsequently water quenched. After the supersaturation process, the slabs (4 mm of thickness) were hot rolled (heating to 1100 °C after every rolling pass) for thickness reduction to 1 mm. After the final pass, the material was quenched in air.

Table 1 – Thermodynamic factors and VEC parameter for the investigated alloy.

ΔH_{mix}, kJ/mol	δ, %	Ω, −	VEC,−
−9.5	4.8	2.0	8.5

Finally, the material was exposure to a temperature range of 650–900 °C for 168 h (7 days).

Tensile flat dog-bone specimens were cut using a wire electric discharge machine with a gauge dimension of $15 \times 3 \times 1$ mm. Tensile tests were conducted via a universal testing machine (INSTRON 5966) at a strain rate of 2×10^{-3} s^{-1} at room temperature. Microstructural investigations were carried out by means of a light microscope (LM–Nikon Eclipse LV150 N), scanning electron microscope (SEM–FEI Versa 3D) with an EDAX electron backscatter diffraction (EBSD) system, and a transmission electron microscope (TEM - FEI Tecnai TF-20 X-TWIN). An EBSD map was collected from a 145 μm × 125 μm area of the hot-rolled sample with a step size of 100 nm. Samples for LM and SEM observations were prepared using standard metallographic techniques and polished using silica oxides with a small addition of malic acid. Next, the samples were etched using a 4 g $CuSO_4$ + 20 ml HCl + 20 ml C_2H_5OH solution for about 2 s. Thin foils for TEM investigations were mechanically prepared and electropolished in a 10-pct. solution of perchloric acid in methanol, at −12 °C and 20 V. It is worth mentioning that the investigated alloy is strongly ferromagnetic, which caused many problems, especially during TEM analysis. It is well known that the Ni-Fe-Co alloys have good ferromagnetic properties [15,18].

The crystallographic structure of the hot rolled material was analyzed by mean of X-ray diffraction with CoKα radiation (Panalytical Empyrean). Hardness measurements were performed by means of an automated hardness tester (Tukon 2500 Willson-Hardness) and Vickers indenter with the applied force of 9.81 N.

3. Results and discussion

Yang et al. presented in [16] the thermodynamic factors required for high-entropy alloys, namely mixing enthalpy (ΔHmix between -15 and -5 kJ/mol), atomic ratio difference parameter δ (≤6.6%), and enthalpy to entropy ratio Ω (≥1.1). In our previous paper [17], we calculated the factors (see Table 1) and our alloy fulfills the above-mentioned requirements. Additionally, the Valance Electron Concentration (VEC) proposed by Guo in [14] (when VEC value: lower than 6.8–BCC structure, higher than 8–FCC structure, and between BCC + FCC structure) was calculated, suggesting that the alloy should have a face-centered cubic structure. The XRD pattern of the investigated alloy after rolling and air quenching is presented in Fig. 1. Only peaks related to FCC solid solution in position 51, 59 and 89° 2θ were recorded, which is in agreement with the theoretical prediction (VEC).

The microstructure of the investigated alloy after rolling is presented in Fig. 2. The grain size in this state varies between 50 and 100 μm. Numerous aging twins (see Fig. 2b-d) and sub-grain structures in the form of intragranular misorientations (see. Fig. 2b) observed in the microstructure seem to correspond with the data presented by Gao et al. [8], related to
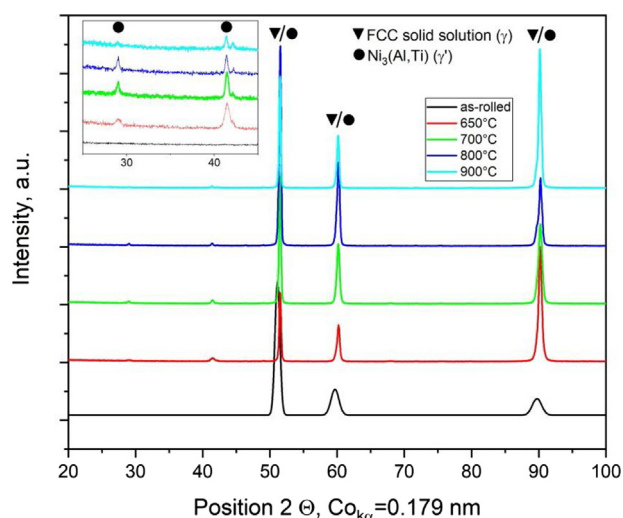
Fig. 1 – XRD pattern of the investigated alloy in as-hot rolled state and after high-temperature exposure to the temperature range of 650–900 °C for 168 h.

problems with achieving equilibrium state in HEA's. Additionally, during air cooling applied after hot rolling, the γ′ (A_3B phase) precipitation occurred. The fine, not exceeding 15 nm in diameter, γ′ precipitates are located uniformly (Fig. 2e,f) throughout the microstructure. It was not possible to confirm the presence of this phase by XRD analysis, due to the size and its small volume fraction of γ′.

The microstructural stability of the hot rolled material was investigated by performing high temperature exposure for 168 h (7 days). LM analysis was used to investigated the grain size and TEM to analyze the precipitation phenomenon. The LM and TEM microstructures and corresponding selected area diffraction patterns are presented in Figs. 3–6. Additionally, in Fig. 6, SEM micrographs of the material after 900 °C exposure is presented. In the temperature range of 650–900 °C, the changes in the grain size are negligible. The growth of individual selected grains exceeding 100 μm can only be observed after exposure to 800 and 900 °C. After exposure to 900 °C, all grain boundaries are decorated by precipitates (Fig. 6a,c).

Exposure to 650 °C caused the growth of the γ′ precipitates, which existed in the material after rolling (Fig. 3b,c). In this state, the size of the γ′ precipitates is between 50 and 200 nm.
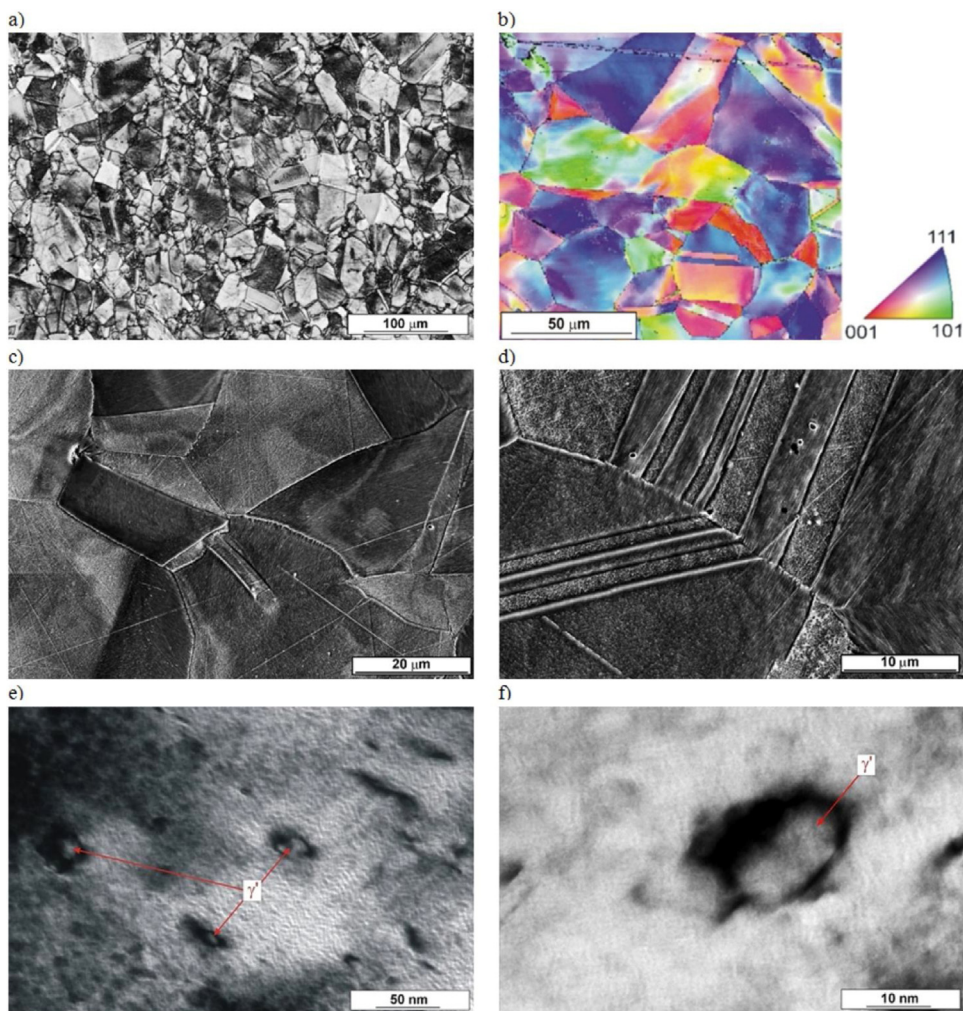
Fig. 2 – Micrographs of the investigated alloy in hot-rolled state. a) grains, LM, b) inverse pole figures, SEM-EBSD c) grains with twins, SEM-SE, d) twins, SEM-SE, e,f) small γ′ precipitates, TEM.
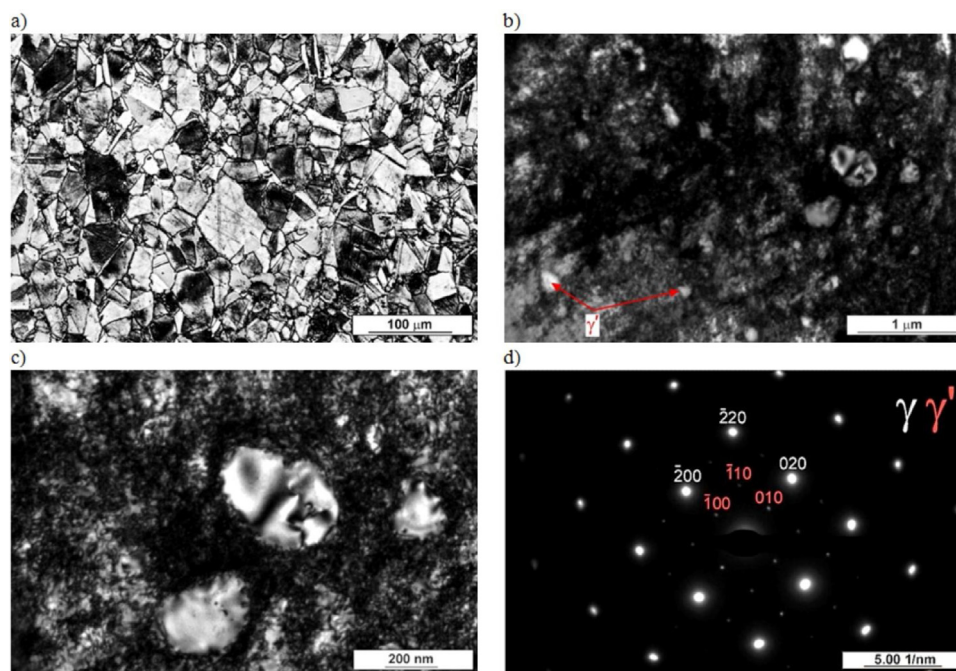
Fig. 3 – Micrographs after exposure to 650 °C for 168 h: a) grains, LM, b,c) γ′ precipitates, TEM, and d) selective diffraction pattern of the area with γ′ precipitates presented in c.

Exposure to 700 °C caused significant changes. Continuous growth of existing after rolling γ′ precipitates, additional continuous precipitation (CP) of γ′ inside the grains (Fig. 4b,c) and discontinuous precipitation at the grain boundaries (Fig. 4b) occurred. Discontinuous precipitation (DP), also known as cellular precipitation, is a precipitation mode, which involves the cellular growth of alternating layers of the precipitated phase and matrix phase behind a moving high-angle grain boundary [19–21]. It can be seen in Fig. 4b that the DP structure occurred to a small extent along the grain boundaries, in the perpendicular direction. The grain boundaries were seen to migrate into a serrated shape due to the tendency of different parts of the same grain boundary to migrate in opposite directions. In our previous paper [22], where a short aging time (4 h) within the same temperature range was applied, we did not observe DP in the investigated alloy, even at a higher temperature, such as 900 °C. Based on literature reviews [21,23,24] and EDS analysis (Fig. 4e) it can be concluded that there were γ′ precipitates interspersed with the γ matrix. γ′ precipitates were additionally enriched in Ni, Co, Ti, and Al. Fe was located only in the γ matrix. According to the results presented in [21], DP observed in the investigated alloy may be a result of high cobalt contents. Based on Ni-Co-Al alloy investigations, the authors concluded that higher cobalt contents results in an increased susceptibility to DP during aging.

Increasing the exposure temperature to 800 °C (Fig. 5) caused an increase in the number of areas where DP occurred, which differentiates HEA's from simple Ni-Co-Al alloys [21,23], where DP usually appears during short time aging. Moreover, in the above-mentioned alloys, with an increase in temperature the susceptibility to CP was greater than DP and above 700 °C, DP did not occur. Authors of [25], suggest that DP will completely invade the microstructure only under conditions,

in which the kinetics of CP are very slow. It seems that, as suggested in [26], there is still much work to be done to fully understand the mechanisms governing DP reactions in multi-component systems.

What is interesting, continuous precipitates of γ′ inside the grains did not grow or the growth was negligible, which contradicts the results presented in [25]. Exposure to 900 °C (Fig. 6) promoted DP. All grain boundaries were decorated with DP with the length over 1 μm in the direction perpendicular to the boundaries. Additionally, DP areas were observed inside the grains (Fig. 6b,c). Probably, if the alloy was exposed for a longer duration, the entire volume of the material would consist of DP, which would be consistent with observation in work [21], where in Ni-Co-Al alloys after aging, DP would constituted throughout the entire volume of the materials. It is worth mentioning that γ′ precipitates existing in the microstructure after hot rolling grew significantly (Fig. 6b). Some of them were larger than 500 nm, whereas continuous precipitates, which were created during exposure to 900 °C slightly increased in comparison to 700 °C (Fig. 6d). Finally, the microstructure of the investigated alloy consisted of γ matrix and three types of γ′ precipitates, i.e. spherical γ′ phase with bimodal distribution within the grains and elongated and DP γ′ phase present at the grain boundaries.

To confirm the above-mentioned changes in the microstructure caused by high-temperature exposure to the temperature range of 650–900 °C for 168 h the XRD analysis was performed (see Fig. 1). Only peaks related to γ (FCC solid solution) and the γ′ phase (Ni₃(Al,Ti)) were identified.

The question is, how does the microstructure affect the mechanical properties of the alloy. The influence of the exposure temperature on hardness, yield strength (YS), and ultimate tensile strength (UTS) measured at 20 °C is presented
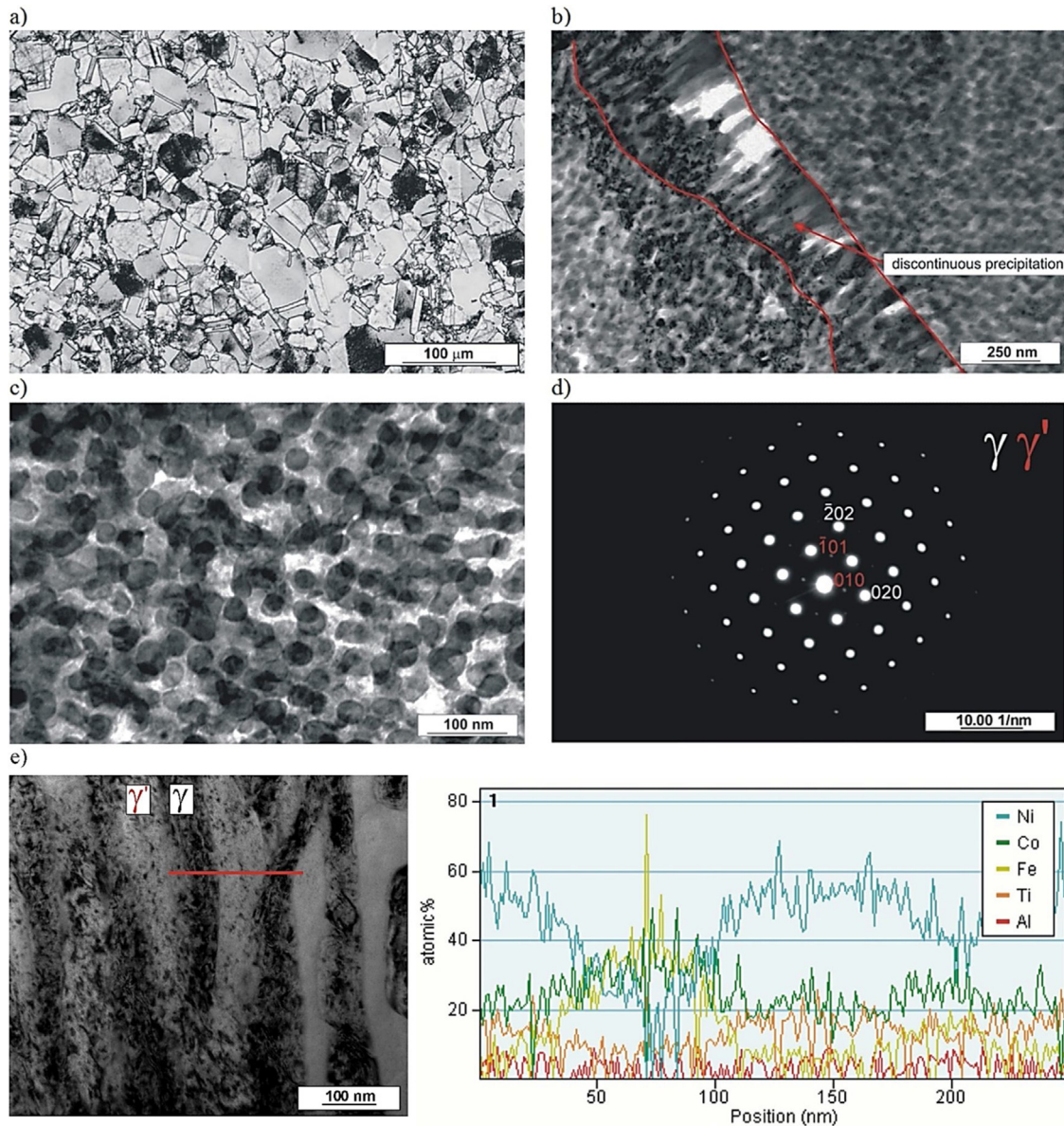
Fig. 4 – Micrographs after exposure to 700 °C for 168 h: a) grains, LM, b) discontinuous precipitation at the grain boundary, TEM, c) γ′ precipitates, TEM, and d) selective diffraction pattern of the area with γ′ precipitates presented in c, e) discontinuous precipitation at the grain boundary with EDS analysis, TEM.

Table 2 – Mechanical properties of investigated alloy in as-rolled state and after high temperature exposure to the temperature range of 650–900 °C for 168 h.			
State	YS [MPa]	UTS [MPa]	UTS/YS
As-rolled	775	1045	1.348
650 °C/168 h	1050	1370	1.305
700 °C/168 h	990	1265	1.278
800 °C/168 h	705	1015	1.440
900 °C/168 h	490	770	1.571

in Fig. 7a and 7b. The data from the tensile tests are presented in Table 2. The highest hardness is exhibited by the sample exposed to 650 °C (455 HV10) and it exceeds the hardness in hot-rolled state by 130 HV. Moreover, CP of γ′ observed after exposure to 700 °C did not cause an increase in hardness (430 HV10). This is related to the growth of γ′ precipitates, which existed in the microstructure after hot rolling and the beginning of DP formation. It is consistent with the hardness decrease to 350 and 260 HV after the exposure of samples to 800 and 900 °C, respectively.

The same relationship was observed in tensile test results. The material after hot rolling presents YS and UTS equal to 775 MPa and 1045 MPa, respectively. Exposure to 650 and 700 °C increased YS up to 1050 MPa and 990 MPa and UTS up to 1370 MPa and 1265 MPa, respectively. The application of higher exposure temperature decreased YS to 490 MPa and UTS to 770 MPa, with a significant increase of elongation for the material exposed at higher temperatures, i.e. ~28% for sample exposed to 900 °C.
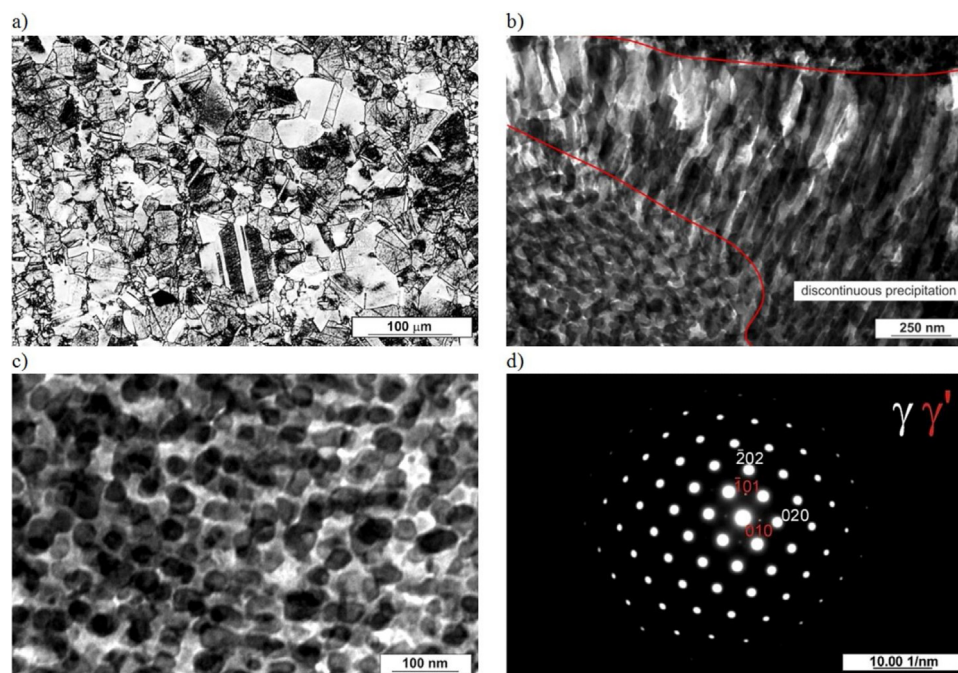
Fig. 5 – Micrographs after exposure at 800 °C during 168 h: a) grains, LM, b) discontinuous precipitation at grain boundary, TEM c) γ′ precipitates, TEM, and d) selective diffraction pattern of area with γ′ precipitates presented in c.

In the case of samples exposed to 650 or 700 °C, the high UTS is related to slip band accumulation in the final step of tensile tests, mainly on γ′ precipitates, which were formed during cooling after hot rolling and have grown during high-temperature exposure. The γ′ precipitates are used to strengthen nickel-based superalloys, where it is well established, so that a dislocation can penetrate the field of γ′ precipitates by either bypassing (the so-called Orowan bypassing mechanism) or cutting the precipitates. The multimodal distribution of γ′ allows superalloys to reach high yield strengths at temperatures even up to 750 °C, while simultaneously maintaining high creep and fatigue life properties [27,28]. In superalloys, which are based on the same elements, Kozar et al. [29], have proposed a model including multimodal γ′ size effects by partially modifying the weak pair-coupling mechanism and introducing size distribution effects in the tertiary γ′. The highest strength is achieved when the secondary γ′ particles are between 150 and 300 nm. After exposure to 650 °C, the size of the γ′ precipitates in the investigated alloy is between 50 and 200 nm, which results in the highest strength. After exposure to 800 and 900 °C, the strength and hardness decreases as a result of continuing γ′ particles growth (the ones, which precipitated during cooling after rolling), as dislocations no longer cut γ′ particles, but bypass them. The γ′ particles precipitated during exposure to 700 °C were too small (less than 50 nm) to play an important role. Based on the above-presented results we proposed the scheme of the microstructure evolution of the investigated alloy during high-temperature exposure and had an influence on mechanical properties of the alloy (Fig. 8).

4.   Conclusions

After hot rolling with air cooling the investigated alloy was not fully supersaturated. The application of air cooling resulted in the precipitation of γ′, which was uniformly distributed within the microstructure. Numerous aging twins and grain misorientations were observed in the microstructure.

High-temperature exposure caused the growth of γ′ particles. At 700 °C and above, additional CP and DP of γ′ phase was observed. After applied heat treatment, the microstructure of the investigated alloy consisted of γ matrix and three types of γ′ precipitates, i.e. spherical γ′ phase with bimodal distribution within the grains and elongated, DP γ′ phase present at the grain boundaries. Higher exposure temperatures tend to favor discontinuous precipitation. After exposure to 900 °C, all grain boundaries were decorated with DP with the length over 1 μm. Moreover, the size of γ′ precipitated during air cooling after hot rolling increased significantly during high-temperature exposure. On the other hand, the difference in size of the γ′ particles precipitated during exposure between 700 °C and 900 °C was negligible. Additionally, the grain size did not significantly change. These factors distinguish the investigated HEA's from superalloys.

The highest hardness and tensile properties were obtained after exposure to 650 °C, which was caused by γ′ precipitates that precipitated during air cooling after hot rolling. Further increase in temperature decreased the mechanical properties.
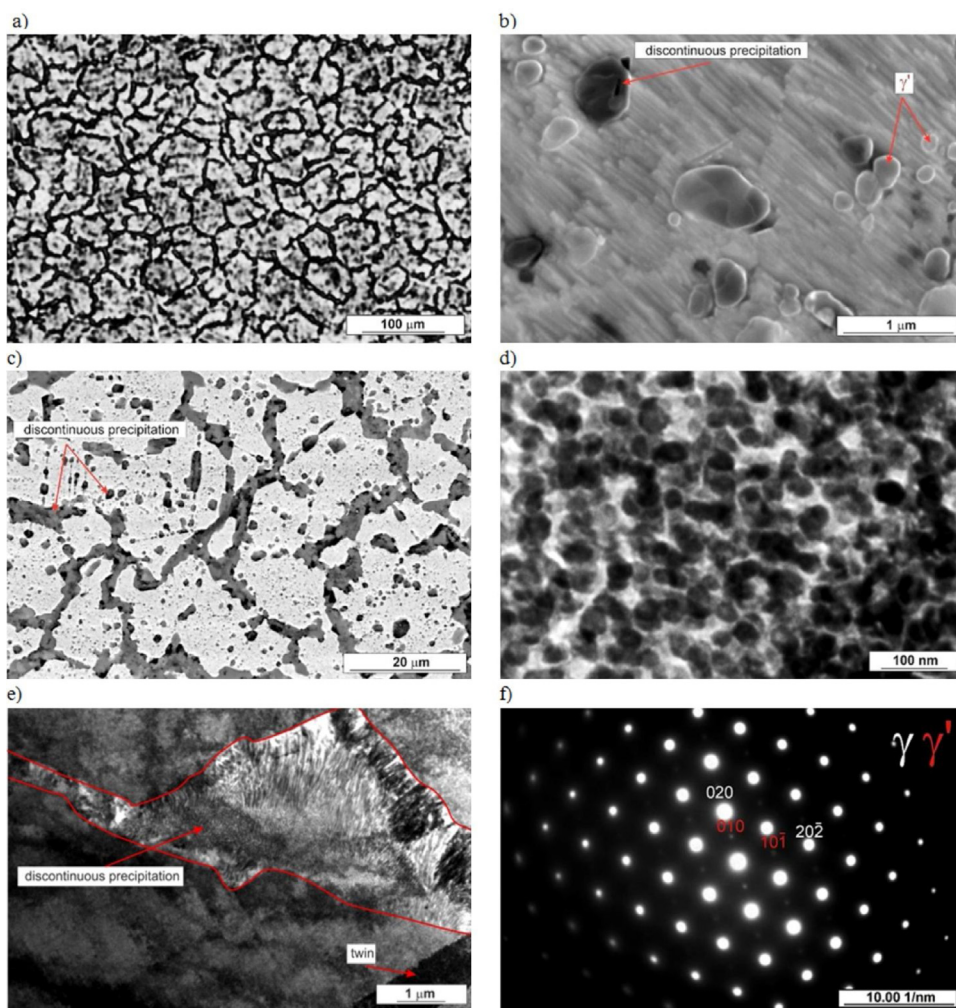
Fig. 6 – Micrographs after exposure to 900 °C for 168 h: a) grains, LM, b) large γ′ precipitates, SEM-SE c) discontinuous precipitation at the grain boundary, SEM-BSE d) continuous γ′ precipitates inside grains, TEM, e) discontinuous precipitation at grain boundary, TEM and e) selective diffraction pattern of the area with γ′ precipitates presented in d.
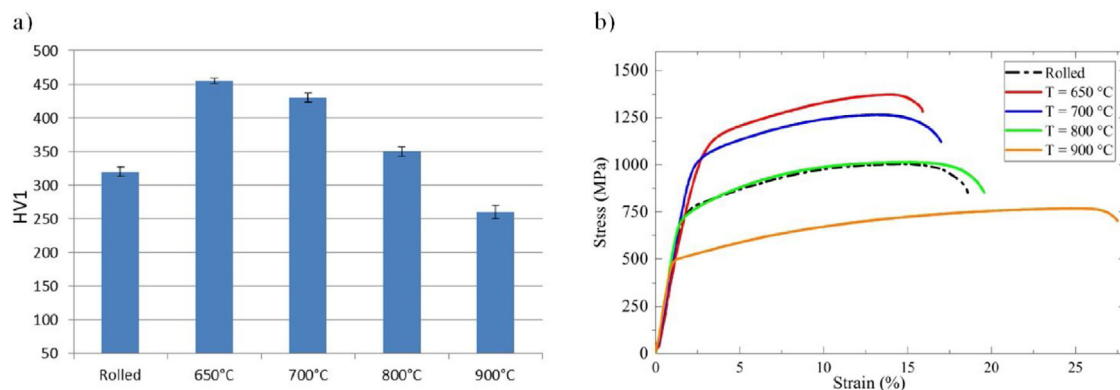
Fig. 7 – a) hardness, and b) engineering stress-strain curves, obtained at room temperature in as-hot rolled state and after high-temperature exposure to the temperature range of 650–900 °C for 168 h.
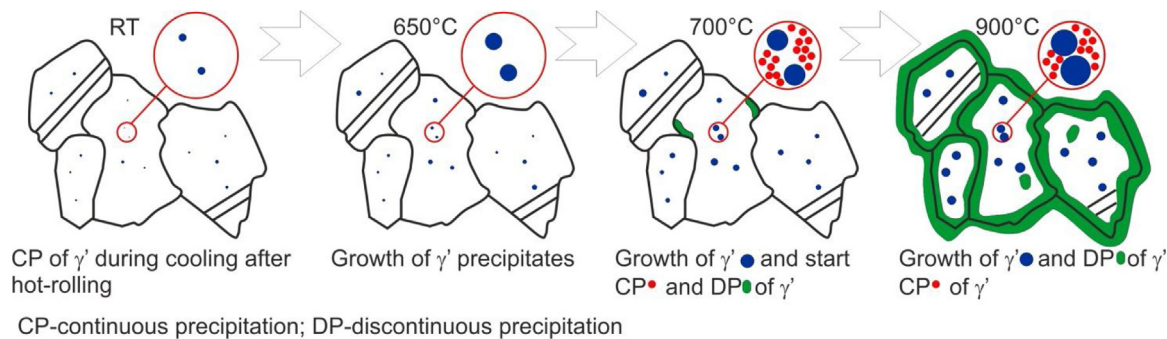
Fig. 8 – Scheme of phase transformation pathway of $Al_5Ti_5Co_{35}Ni_{35}Fe20$ high-entropy alloy from as-rolled to annealed at 900 °C for 168 h, where DP-transformed regions gradually transform to near-equilibrium microstructure along with CP.

Data availability

The raw/processed data required to reproduce these findings cannot be shared at this time as the data also forms part of an ongoing study.

REFERENCES

[1] Callister WD Jr. Materials science and engineering: an introduction. USA: John Wiley & Sons; 2003.

[2] Askeland DR, Wright WJ. The science and engineering of materials. Seventh edition Cengage Learning; 2016.

[3] Metals Handbook. Properties and Selection: Nonferrous Alloys and Special-Purpose Materials was published in 1990 as Volume 2 of the 10 Edition Metals Handbook. With the second printing (1992), the series title was changed to ASM Handbook.

[4] Metals Handbook. Properties and Selection: ferrous Alloys and Special-Purpose Materials was published in 1990 as Volume 2 of the.

[5] Cantor B. Multicomponent and high entropy alloys. Entropy 2014;16:4749–68.

[6] Yeh JW, Chen SK, Lin SJ, Gan JY, Chin TS, Shun TT, et al. Nanostructured high-entropy alloys with multiple principal elements: novel alloy design concepts and outcomes. Adv Eng Mater 2004;6:299–303.

[7] Yeh JW, Chen YL, Lin SJ, Chen SK. High-entropy alloys–a new era of exploitation. Mater Sci Forum 2007;560:1–9.

[8] Gao MC, Yeh JW, Liaw PK, Zhang Y, editors. High-entropy alloys. Fundamentals and applications. Springer; 2016., http://dx.doi.org/10.1007/978-3-319-27013-5.

[9] Stepanov ND, Shaysultanov DG, Ozerov MS, Zherebtsov SV, Salishchev GA. Second phase formation in the CoCrFeNiMn high entropy alloy after recrystallization annealing. Mater Lett 2016;185:1–4, http://dx.doi.org/10.1016/j.matlet.2016.08.088.

[10] Bracq G, Laurent-Brocq M, Perrière L, Pirès R, Joubert JM, Guillot I. The fcc solid solution stability in the Co-Cr-Fe-Mn-Ni multi-component system. Acta Mater

2017;128:327–36, http://dx.doi.org/10.1016/j.actamat.2017.02.017.

[11] Zhu ZG, Ma KH, Yang X, Shek CH. Annealing effect on the phase stability and mechanical properties of (FeNiCrMn)(100−x)Cox high entropy alloys. J Alloys Compd 2017;695:2945–50, http://dx.doi.org/10.1016/j.jallcom.2016.11.376.

[12] Tsai MH, Yeh JW. High-entropy alloys: a critical review. Mater Res Lett 2014;2:107–23, http://dx.doi.org/10.1080/21663831.2014.912690.

[13] Miracle DB, Senkov ON. A critical review of high entropy alloys and related concepts. Acta Mater 2017;122:448–511, http://dx.doi.org/10.1016/j.actamat.2016.08.081.

[14] Guo S, Ng C, Lu J, Liu CT. Effect of valence electron concentration on stability of fcc or bcc phase in high entropy alloys. J Appl Phys 2011;109:103505, http://dx.doi.org/10.1063/1.3587228.

[15] Liu X, Zangari G, Shen L. Electrodeposition of soft, high moment Co–Fe–Ni thin films. J Appl Phys 2000;87:5410, http://dx.doi.org/10.1063/1.373359.

[16] Yang X, Zhang Y. Prediction of high-entropy stabilized solid-solution in multi-component alloys. Mater Chem Phys 2012;132:233–8, http://dx.doi.org/10.1016/j.matchemphys.2011.11.021.

[17] Górecki K, Bała P, Kozieł T, Cios G. Necessary thermodynamics factors to obtain simple solid solutions in high-entropy alloys from the Al-Ti-Co-Ni-Fe system. Arch Metall Mater 2017;62:2141–5, http://dx.doi.org/10.1515/amm-2017-0316.

[18] Osaka T. Electrodeposition of highly functional thin films for magnetic recording devices of the next century. Electrochim Acta 2000;45:3311–21, http://dx.doi.org/10.1016/S0013-4686(00)00407-2.

[19] Turnbull D. Theory of cellular precipitation. Acta Metall 1955;3:55–63.

[20] Cahn JW. The kinetics of cellular segregation reactions. Acta Metall 1959;7:18–28.

[21] Davies C, Nash P, Stevens R, Yap L. Precipitation in Ni-Co-Al alloys. J Mater Sci 1985;20:2945–57.

[22] Górecki K, Bała P, Bednarczyk W, Kawałko J. Cryogenic behaviour of the Al5Ti5Co35Ni35Fe20 multi-principal component alloy. Mater Sci Eng A 2019;745:346–52, http://dx.doi.org/10.1016/j.msea.2019.01.001.

[23] Zhoua Y, Zhou F, Martins JMR, Nash P, Wang J. The effect of discontinuous γ' precipitation on the mechanical properties of Al-Co-Ni alloys. Mater Charact 2019;151:612–9, http://dx.doi.org/10.1016/j.matchar.2019.04.003.

[24] Zhou Y, et al. Phase equilibria in the Al-Co-Ni alloy system. J Phase Equilib Diffus 2017;38:630–45, http://dx.doi.org/10.1007/s11669-017-0586-z.

[25] Robson JD. Modeling competitive continuous and discontinuous precipitation. Acta Mater 2013;61(20):7781–90, http://dx.doi.org/10.1016/j.actamat.2013.09.017.

[26] Spadottoa JC, Dille J, Watanabe M, Solórzano IG. Grain boundary precipitation phenomena in an alloy 33 (Cr-Fe-Ni-N) subjected to direct-aging treatments (700 °C and 900 °C). Mater Charact 2018;140:113–21, http://dx.doi.org/10.1016/j.matchar.2018.03.046.

[27] Reed R. The Superalloys: Fundamentals and Applications. Cambridge: Cambridge University Press; 2006.

[28] Unocic R, Viswanathan G, Sarosi P, Karthikeyan S, Li J, Mills M. Mechanisms of creep deformation in polycrystalline Ni-base disk superalloys. Mater Sci Eng A 2008;483: 25–32.

[29] Kozar R, Suzuki A, Milligan W, Schirra J, Savage M, Pollock T. Strengthening mechanisms in polycrystalline multimodal nickel-base superalloys. Metall Mater Trans A 2009;40:1588–603, http://dx.doi.org/10.1007/s11661-009-9858-5.